Petroleum Res. J. Vol. 15 (2003): P. 1–22, 19 Figs.

A Qualitative Structural Evaluation of Jabal Az Zalmah Area, Al-Kufrah Basin: Integration of Structural and Aeromagnetic Mapping

Amin A. Sherif*

التقييم النوعي للتراكيب الجيولوجية لجبل الظلمة، حوض الكفرة: التكامل بين التخريط التركيبي والمغناطيسي

الأمين عبد الله الشريف

من خلال الدراسة الحقلية و تحليل الصور الجوية للمنطقة الشمالية–الشرقية من حوض الكفرة في جنوب شرقي ليبيا، تم تجميع خريطة تكتونية وإعداد دراسة تحليلية لحركية مجموعة من التراكيب المتوازية الأضلاع. أظهرت هذه الدراسات فئات الصدوع الرئيسية التالية:

صدوع انزلاق – مضرب يمينية ذات اتجاه شمالي – غربي.

صدوع انزلاق – مضرب يسارية ذات اتجاه شمالي شرقي.

صدوع شرق– غرب كفئة فرعية من الفئتين السابقتين.

أما الصدوع الواقعة في إتجاه شمال–جنوب فهي في الأساس صدوع عادية ممثلة بفئة مخسفات واضحة المعالم في نظام تدريجي يميني. هذه الفئات من الصدوع أظهرت نظام انحراف يساري في اتجاه شمال شرق، وبعرض 30 كم، مكون من أربع نطاقات متساوية تقريباً في العرض، كل نطاق منها يحصر أو يتحكم في توزيع الصدوع الشمالية–الغربية. المنخسفات الشمالية–الجنوبية، ذات ترسبات من العصر الأوردفيشي العلوي، تحدد بداية نظام الانحراف عند العصر الكمبري الأخير أو الأوردوفيشي الأول، لأن هذه المنخسفات توقف أو تحصر أو تتحكم في إنتشار جميع فئات الصدوع في المنطقة.

إن صخور القاعدة التي تم دراسة هيئتها من خلال خريطة مغناطيسية جوية، أكدت تواجد نظام الإنحراف، حيث أن وسط نظام الانحراف المقترح، كما يظهر على السطح، يتوافق مع وادي سحيق في إتجاه شمال–شرق على الخريطة المغناطيسية. كما تم دراسة مجموعة من الشاذات المغناطيسية مقابل النموذج الحركي للمنطقة، وتبين أن هذه الشاذات تتوافق مع نظام الإنحراف المقترح، وذلك من خلال تراكيب متكشفة على السطح.

Abstract: *The compilation of a fault map from field work and photo interpretation for part of the north-eastern flank of Al Kufrah Basin in south-east Libya, together with the kinematic analyses of several rhomboid structures, showed the following major fault sets: dextral NW strike-slip faults; sinistral NE strike-slip faults; and EW faults as subsidiary sets of either the NW or NE trends. The NS trend, mainly as normal faults, is represented by a north-south, right-stepping set of well-defined en echelon grabens. These fault sets revealed a NE sinistral wrench system, about 30 km-wide, made up of four belts of almost equal width, each delimiting or controlling the distribution of the NW faults. The NS grabens, which are filled with Upper Ordovician sediments,*

* Department of Geology, Faculty of Science, Al Fatah University, Tripoli-Libya.

mark the initiation of the wrench system as early as Late Cambrian or Early Ordovician, because they control, restrict, or confine the distribution of all the other fault sets in the area.

The basement configuration as interpreted from a total intensity aeromagnetic map for the area confirmed the existence of this wrench system, where the median of the proposed wrench system at the surface coincides with a NE-trending deep valley on the magnetic map. Several magnetic anomalies were tested against the kinematic model for the area and were found to comply with the proposed wrench system, with identical structural manifestations on the surface.

INTRODUCTION

A preliminary geological map is presented here as part of the geological mapping project for Jabal Al Qardabah Sheet (Fig. 1), one of the mapping projects carried out by the Industrial Research Centre (IRC). It is part of Jabal Az Zalmah area, on the north-eastern flanks of Al Kufrah Basin, SE Libya. The geologic map (Fig. 2) represents an area of about 5000 Km^2, and comprises eight 15-minute sheets.

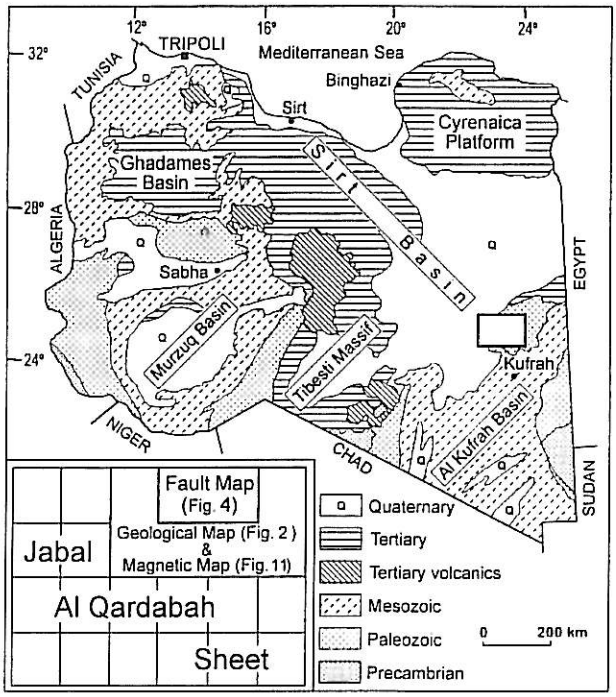

Fig. 1. Index map to the geology of Libya showing the location of Jabal Al Qardabah Sheet on the NE flanks of Al Kufrah Basin. Inset shows the location of the geological map (Fig. 2) fault map (Fig. 4) and magnetic map (Fig.. 11) with respect to Jabal Al Qardabah Sheet.

Structural photo interpretation was carried out using eight strips of stereo-pairs having 60% overlap and 30% sidelap at a scale of 1: 40,000. Each 15-minute sheet is covered by three to four north-south-running strips of aerial photographs, seven to ten overlapping photos per strip. A fault map for two of these sheets (Fig. 4) was compiled from the interpretation of aerial photographs and fieldwork. Both of these maps will be studied in relation to each other to investigate any association between the distribution of the stratigraphic units and the tectonic setting of the area.

A third map, a residual total intensity aeromagnetic map (Fig. 11), will be qualitatively analysed, and later interpreted in terms of the structural and stratigraphic observations derived from the fault map and the geological map, respectively. The magnetic map covers exactly the same area as that covered by the geological map (see Fig. 1). This should help in making a three-dimensional correlation between the surface geology and the basement "topography". Based on such correlation, a tectonic model for the study area will be proposed.

STRATIGRAPHY

The author was directly involved in the mapping of Jabal Al Qardabah Sheet through the structural analyses of the area, while Mr. Yousif A. Shagroni of the Industrial Research Centre established the stratigraphy for the area. The participation of the present author in the capacity described allowed access to the stratigraphy of the area. A synopsis of the stratigraphy is presented here as personal communication from Mr. Shagrouni (Fig. 3).

The north-eastern outcrops (Az Zalmah area) of Al Kufrah Basin is represented mainly by Palaeozoic and Cretaceous rocks. The Cretaceous rocks are not shown on figure 2 because of their restricted outcrops and the scale limitations of the map. The whole sequence is made up of clastic rocks (Fig. 3). Unlike the south-eastern and south-western outcrops of Al Kufrah Basin, this poriotn of the basin is almost barren of any igneous or metamorphic exposires, save for a basaltic ring structure within the central west of Jabal Al Qardabah Sheet, at 25°37'00" N, 22°47'00" E (beyond the western limits of figure 2).

Within the area of figure 2, the Lower Palaeozoic sequenes (Cambrian to Lower Devonian) almost follows the same lithostratigraphic subdivisions found in Murzuq Basin. The deviations are: 1) the missing of Hawaz Formation (Middle Ordovician), and 2) the

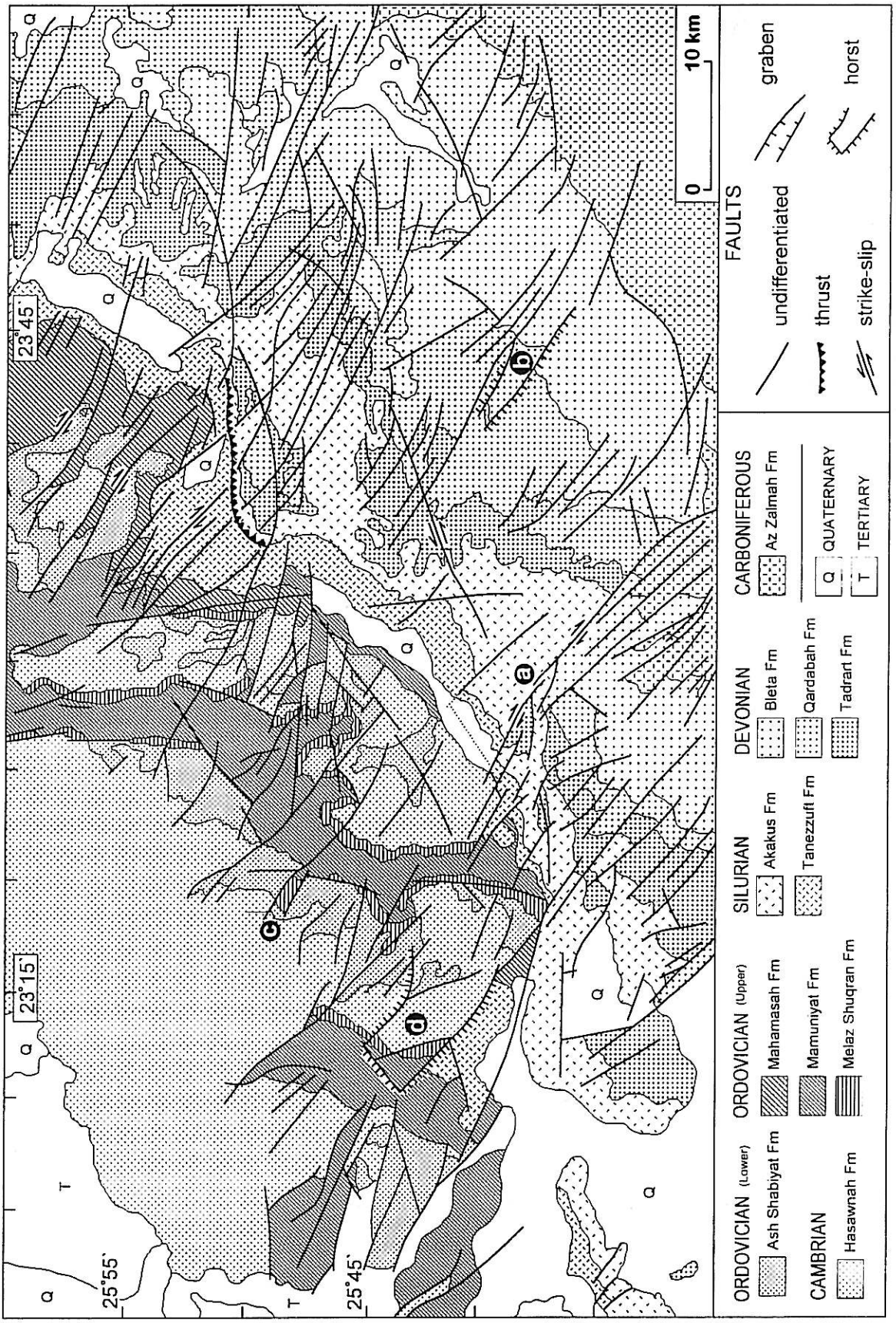

Fig. 2. Geological map for part of Jabal Al Qardabah Sheet (Yousif A. Shagroni, personal comunication). The magnetic map (Fig. 11) covers the same area to facilitate correlation between surface geology and basement (see index map Fig. 1). Circled labels a-d refer to structures on Fig. 8.

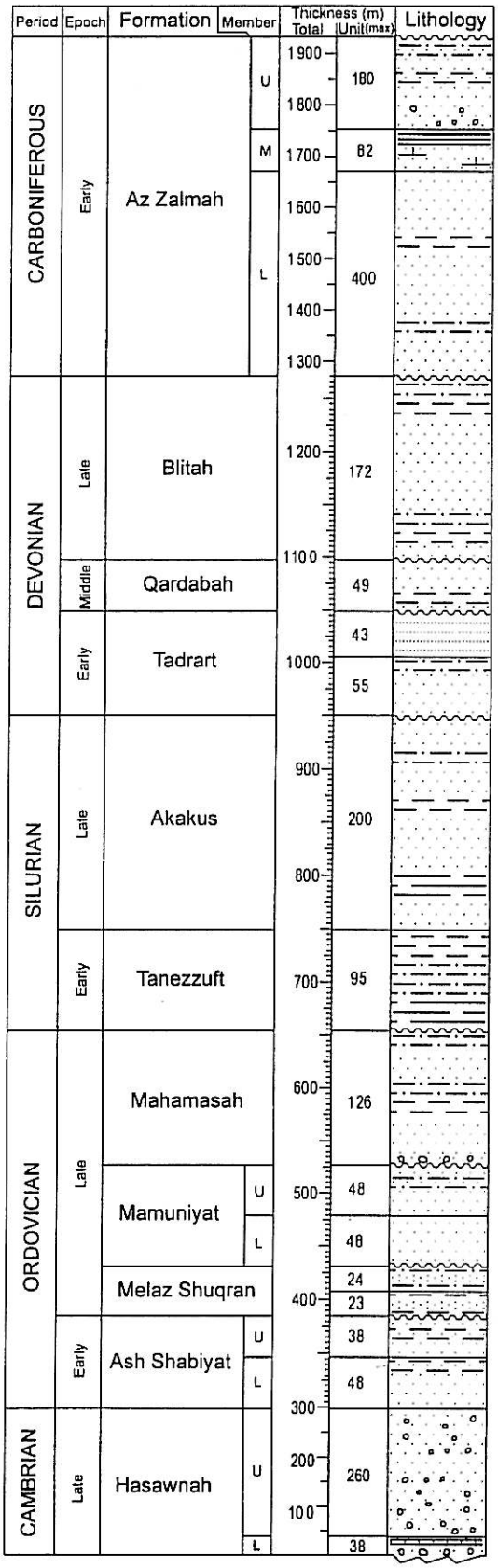

Fig. 3. Stratigraphy of Az Zalmah area (Yousif A. Shagroni, personal comunication). Thickness for individual units represent maximum of composite sections. Note variation of thickness scale.

addition of Mahamasah Formation (Upper Ordovician).

For the Upper Palaeozoic (Middle Devonian to Carboniferous), Al Kufrah Basin was separated from Murzuq Basin by the Tibesti-Sirt Uplift beginning in Middle Devonian, or post Tadrart Formation (Klitzsch, 1966, Bellini and Massa, 1980). This isolation created a different style of deposition unique to Al Kufrah Basin, which has a lithology different from that found in Murzuq Basin.

Cambrian

Hasawnah Formation (Late Cambrian)

Lower Member (38 meters): Made up of several fining-upward cycles. The lower part is generally coarse- to medium-grained sandstone, well rounded and cross-bedded, conglomeratic at lowermost levels (base is not exposed in the area). The cycles in the middle part start with thickly-bedded, coarse-grained sandstone, and terminate with thinly-bedded, fine- to medium-grained sandstone with intercalations of silt and very fine-grained sandstone. The upper part is represented by four fining-upward cycles that grade from coarse-to medium- to fine-grained sandstone, and terminate with micaceous shale interbeds.

Upper Member (260 meters): Represented by fining- and thinning-upward cycles of coarse- to medium-grained, cross-bedded sandstones. The cycles within the lower part of this member are mostly conglomeratic at their lower levels, becoming lenses of imbricated conglomerate upwards, while these same cycles are terminated by ferruginous, very fine-grained sandstone and siltstone. The uppermost 15 meters of the lower part are rich in *Arthrophycus* and *Crusiana*. The cycles within the upper part are sharp-based and terminate with medium- to fine-grained sandstone. The uppermost 40 meters of the Upper Member are rich in *Tigillites*.

Ordovician

Ash Shabiyat Formation (Early Ordovician)

Lower Member (10-48 meters): Fining- and thinning-upward cycles of coarse- to medium-grained, *Tigillite*-bearing, kaolinitic sandstone. At different levels, this lithology is sometimes intercalated with cross-bedded sandstone. The cycles are often terminated by about 20 cm of bluish-green clay.

Upper Member (38 meters): Fine-grained, thinly-bedded sandstone containing *Arthrophycus*, with silt intercalations occasionally alternating with interbeds of fine- to medium-grained, cross-bedded sandstone.

Melaz Shuqran Formation (Late Ordovician)

Lower Part (23 meters): Olive-green claystone, gypsiferous in the lower 6 meters, intercalated in intervals by fine-grained sandstone and micaceous siltstone, as laminated and/or rippled bedding or as flakes.

Upper Part (0-24 meters): Very fine-grained sandstone and siltstone, in the form of rippled bedding, with intercalations of claystone.

Mamuniyat Formation (Late Ordovician)

Lower Member (48 meters): Sandstones with a wide spectrum of grain size ranging from fine to medium to cobble, as well as varying textures from immature to mature within a very close distance, sometimes as few as tens of meters. Bedding thickness is also in the range of 0.4 to 2 meters. Furthermore, primary sedimentary structures within individual beds are extremely deformed: laminated beds are highly convoluted; cross-bedded sets develop overturned structures; and slump-like structure, as well as massive and poorly defined internal structures are observed.

Upper Member (48 meters): In contrast with the lower Member, the upper Member is thinly to medium, evenly bedded, mostly micaceous, well sorted, medium to coarse-grained sandstone. As for the sedimentary structures, the Upper Member has horizontal or gently dipping lamina and/or rippled bedding. Furthermore, the upper part is found to be intercalated with micaceous, silty, very fine-grained sandstone containing few poorly preserved moulds of brachiopods.

Mahamasah Formation (Late Ordovician)

Made up of coarsening-upward cycles–either thinning-upward or thickening-upward–distributed among four levels. Each of these levels seem to be deposited in a distinctive structurally controlled setting.

Level 1 (36 meters): The oldest level, made up of four coarsening-upward, thinning-upward cycles, each starting with claystone, followed by fine- to medium- to coarse-grained sandstone, and ending with medium- to coarse-grained, conglomeratic sandstone.

Level 2 (5.5-12.5 meters): Made up of three coarsening-upward, thinning-upward cycles of claystone, followed by fine- to medium-grained, or fine-grained, subangular sandstone..

Level 3 (50 meters): Represented by one coarsening-upward cycle. This level has two distinctive thickening-upward cycles with an intervening thinning-upward cycle. From bottom, it is made up of: claystone; intercalations of clay, silt, and fine-grained sandstone; fine- to medium-grained sandstone; and fine- to medium-grained, subangular sandstone that starts with cross-bedding and ends with lamination.

Level 4 (22 meters): The youngest level, with two coarsening-upward, thinning-upward cycles. In sequence, these cycles are represented by: claystone; siltstone; fine-grained sandstone; fine- to medium-grained sandstone; and medium- to coarse-grained sandstone.

Silurian

Tanezzuft Formation (Early Silurian)

Mostly represented by coarsening-upward cycles of variable thickness, with an overall thickness ranging between 20 and 95 meters (more than ten cycles at maximum thickness). These cycles start with argillites having variable shades of blue and green, and terminates with cross-rippled, micaceous siltstone. They range in thickness between 1.5 and 5.5 meters, with no preferential thickness trend. Within the last few meters of Tanezzuft Formation, the cycles become fining-upward, mostly made up of brownish green gypsiferous argillites, with flakes and very thin lenticular beds of siltstone. It is worth mentioning that the older levels of this unit are found to fill, progressively, the deepest palaeosites.

Akakus Formation (Late Silurian)

Represented by more than 30 coarsening-upward cycles, ranging in thickness between 1.5 and 10.5 meters, while the recorded thickness for the whole

unit is between 80 and 200 meters. The lower ½ of the formation is mostly made up of argillites, followed by silt, and ending with fine- to very fine-grained, cross-laminated and micaceous sandstone. The cycles within the upper ½ of the formation are mostly terminated by large lenses (more than 30 meters long) of thinly to medium-bedded and flaced, fine-grained sandstone. Among the sedimentary structures found within the upper half of Akakus Formation: convoluted bedding, wrinkled ripples, mud cracks, wavy bedding, and double-crested ripples. The upper ¾ of Akakus Formation become progressively rich in trace fossils: *Crusiana*, *Arthrophycus*, and *Tigillites*.

Within the study area, the Devonian is represented by Tadrart Formation, Qardabah Formation, and Blitah Formation (Fig. 3). The Qardabah Formation is a new unit introduced here, having no equivalent in Murzuq Basin, nor has it been identified in Al Kufrah Basin. These three formations represent different depositional systems, separated by clear and sharp erosional surfaces.

Devonian

Tadrart Formation (Early Devonian)

Lower Part (28-55 meters): Coarsening-upward, fining-upward cycles of fine- to medium-grained, subangular, cross-bedded sandstone, with interlevels of fine-grained, micaceous, cross-bedded sandstone. This lithology is found to be interfingering–within the upper half of this interval–with fine-grained sandstone and siltstone, having clay intercalations and containing *Arthrophycus*.

Upper Part (0-43 meters): Sandstone: fine- to medium-grained, subangular, cross-bedded or laminated, Tigillite-bearing. This interval represents one thinning-upward sequence.

The maximum recorded thickness for Tadrart Formation was 83 meters.

Qardabah Formation (Middle Devonian)

The main constituency of this formation is either cross-bedded sandstone or *Tigillite*-bearing sandstone, the latter being more dominant. The texture for these sandstones is coarse- to very coarse-grained within the lower and upper levels of this formation, while it is fine- to medium-grained in the middle levels, with a well rounded texture throughout the sequence. The cross-bedded sandstones sometimes start with conglomerates, while in others they terminate with lamination sets. On the other hand, the fine- to medium-grained sandstones sometimes terminate with siltstones and claystones. The uppermost levels of this formation contain *Zoophycus*. The recorded thickness for Qardabah Formation is between 38 and 49 meters.

Blitah Formation (Late Devonian)

Generally representing coarsening- and thickening-upward cycles. Each cycle starts with claystone, followed by claystone with intercalations of lenticular siltstone and very fine-grained micaceous sandstone, and terminating with fine- to very fine-grained sandstone with clay parting. The sandstones of some of these cycles are cross-bedded, while some other cycles bare mud cracks at their topmost levels. The base of this formation starts everywhere with light bluish-green muds, while it is terminated by bluish-green claystones found as intercalations and/or lenticulations with very fine-grained sandstone. The formation is abound with *Zoophycus*, with minor *Tigillites* and *Chondrites*, while *Brachiopod* moulds are found at the topmost levels. The recorded thickness for Blitah Formation is between 163 and 172 meters.

Carboniferous

Az Zalmah Formation (Early Carboniferous)

Lower Member (400 meters): Fine- to medium- to coarse-grained sandstone. Often as cross-bedded and in fining-upward cycles. At different levels the fine sandstones are intercalated with siltstone and claystone. Rootlets and *Lepidodendrons* are also found at different levels, mostly associated with mud cracks. *Zoophycus* and *Tigillites* are the main trace fossils.

Middle Member (82 meters): Mostly very fine-grained sandstone as lenticular bedding. Burrows and rootlets are found as intervals at different levels, as well as intervals of argillites and claystone. Upper part has intercalations of siltstones, argillites, and shale. Topmost levels are represented by fine- to medium- to coarse-grained sandstone with shale intercalations.

Upper Member (180 meters): Sandstones with grain size ranging between very fine to very coarse,

being microconglomeratic at lower most levels. Lower part found as cross-bedded, while the middle part is calcareous or micaceous. The upper part is found as fining- or coarsening-upward cycles, the latter being more dominant. Throughout this part, the fine- to very fine-grained levels of either of these cycles is most often associated with clays as flakes, partings, or intercalations.

STRUCTURAL FRAMEWORK

Two 15-minute sheets, bounded by longitudes 23°15'00"-23°45'00" E and latitudes 25°45'00"-26°00'00"N were selected for structural interpretation. This area was found to include most of the Palaeozoic sequence, from Cambrian in the north-west to Devonian in the south-east (Fig.2).

The structural interpretation involved folds, faults and joints, but emphasis was on all linear or semi-linear structural features of any length, that appear to represent faults or joints. These fractures were either explicit or inferred from features such as a break in topography or an offset in drainage, a change in tone, or from the alignment of hills along a semi-linear trend.

Throughout the area covering Jabal Al Qardabah Sheet, most of the fault planes which were visited in the field show a very clear horizontal component of displacement, as expressed by either horizontal grooves or slickensides. These strike-slip faults are also very clearly seen on topographic planes, with offsets ranging between few meters to tens of meters. Strike-slip faults were most often found in *en echelon* sets having either NW or NE orientation, while NS and EW faults were most often confined within well defined, fault-bounded structures. In the field, NS and EW faults generally show negligible vertical displacement, much less horizontal displacement, despite the fact that these fault sets represent very long fault lines or lineaments, sometimes exceeding 20km.

The data gathered from the structural photo-interpretation and supported by field checks was transferred onto controlled mosaics at a scale of 1:50,000, thus resulting in a controlled *fault map* (Fig. 4, see Fig. 1 for location). The fault map was then filtered manually through a template to obtain separate *trend maps* for every major trend, namely, NS, EW, NE, and NW (Fig. 6). The devised template (centre of figure 6) allowed the picking of any fault within a specified azimuth range for any particular

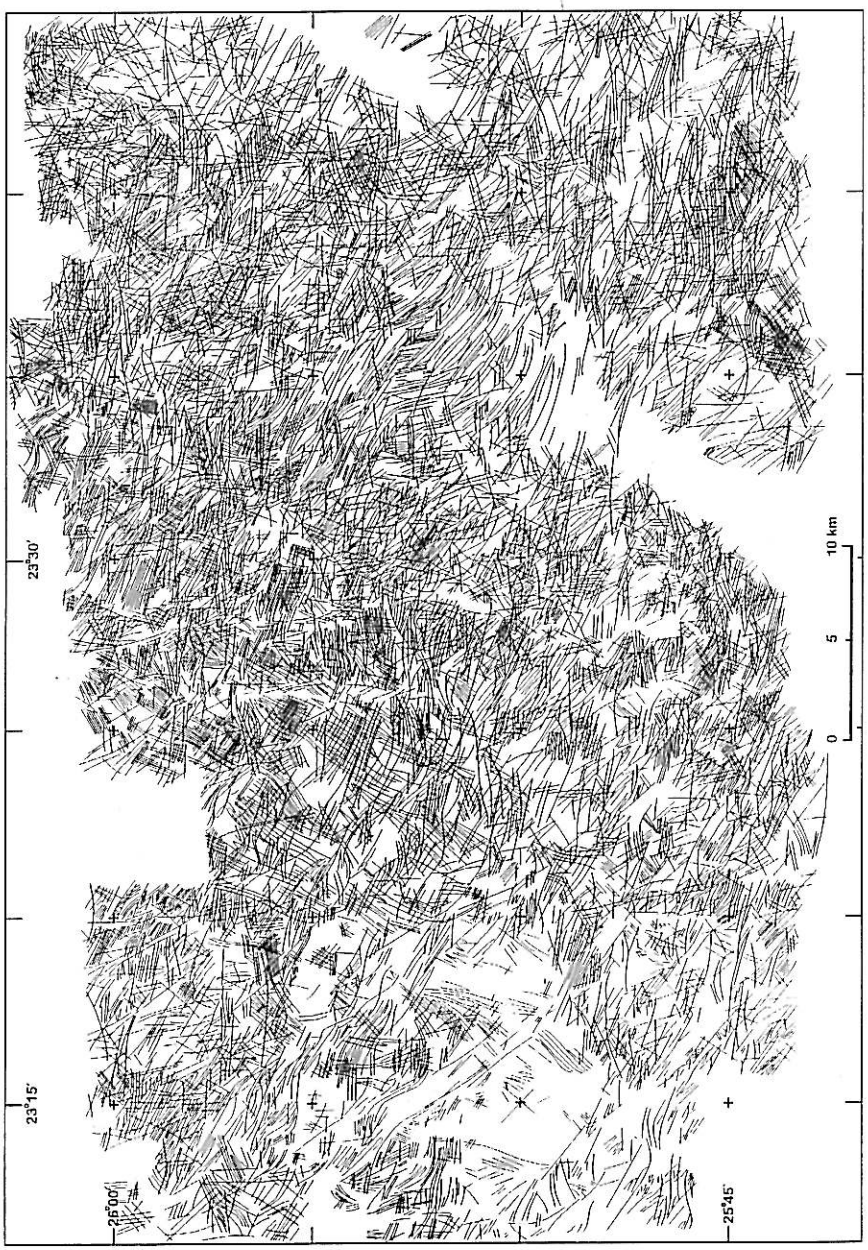

Fig. 4. Fault map of part of Jabal Al Qardabah Sheet, NE Al Kufrah Basin, compiled from photinterpretation of stereoscopic aerial photographs. See Fig. 1 for location.

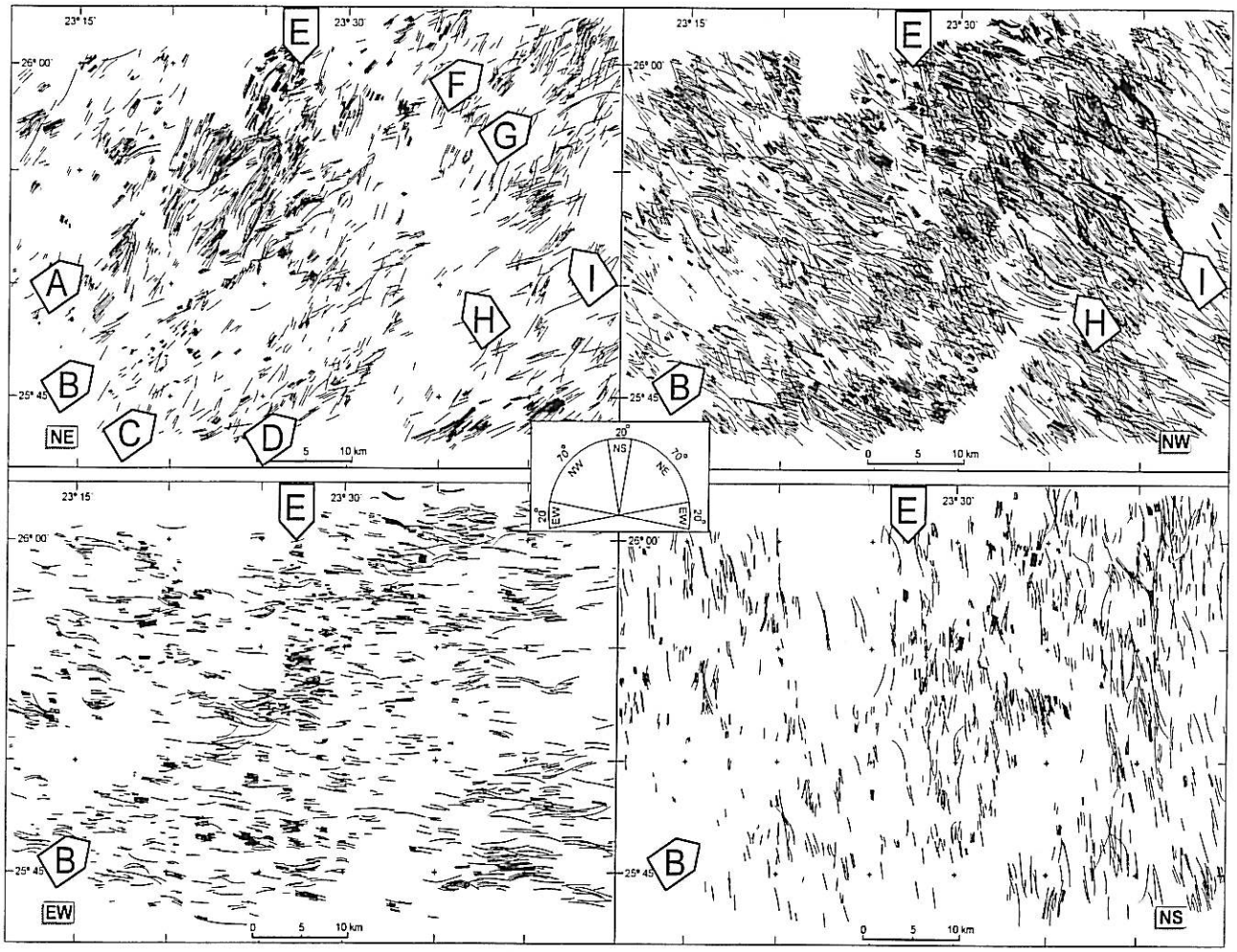

Fig. 5. Major trend maps filtered from fault map (Fig. 4) through the template shown in centre. Labels A to I represent major fault sets (see text for description).

trend. Thus, the NS and EW trends were both given an azimuth range of 20°, while the NW and NE trends were given a 70° azimuth range. The NW and NE trends, having a wide angle range, were further separated into NNW, WNW, and NNE, ENE, respectively (Fig. 6).

The majority of faults in the area are not clear straight faults, rather they are curved or bent. For that the manual approach for filtering the eight trend maps (Figs. 5 and 6) was favoured because it allowed, for example, the picking of a bent northwest-trending fault to be included in both the NW and NS trend maps. Similarly, and for the same fault, it could also be included in both the NNW and WNW trend maps.

Fault Sets

Several fault sets can be traced at once on all eight trend maps of figures 5 and 6. These are either found as linear fault sets or as clusters of faults. The description of these fault sets follows.

Fault Sets A, B, C, and D

All four of these sets are NE linear sets, therefore they are all explicitly seen on the NE trend map in figure 5 and on the ENE trend map in figure 6. However, the NNE trend, and while it is a subset of the NE trend, shows no trace of these fault sets, except for *fault set A* where it is manifested as a separator between the two main clusters of faults seen on the NNE trend on figure 6. This indicates that all four of these fault sets belong to the ENE trend.

While *fault set B* is barely seen on the NNE trend map, its manifestation and control on all the other trend maps, without exception, is very conspicuous. In all of these maps, the fault population is much higher east of *fault set B*. This is particularly seen

on the EW trend map (Fig. 5) and the NNW trend map (Fig. 6), where the faults stop abruptly along the trace of *fault set B* and to the east of it. This same effect is also found on the NW and WNW trend maps, even though these two trends have the highest and evenly distributed fault population in the area.

With its impact on all the trends in the area, *fault set B* is not just made up of a single throughgoing set of faults, rather it is made up of conjugate sets of faults (see NE trend, Fig. 5). This feature is not found along the other fault sets described so for, which suggests that *fault set B* could represent the median of a wide fault zone (about 30 km wide) encompassing all the NE fault sets described above.

Fault Set E

The control of this north-south fault set is also seen in all the trend maps, yet it is only partially seen on the NS trend map (Fig. 5). The EW trend map shows a cluster of east-west faults confined within a narrow zone running north-south and in the path of *fault set E* (Fig. 5). A direct comparison between the EW and NS trend maps reveals that *fault set E* is not just one fault set but in fact it is made up of two NS parallel fault sets, with an intervening distance of about 4 km. Therefore, the confinement of EW faults is directly related to *fault set E*, which makes the latter more like a graben defined by two NS fault sets.

The effect of *fault set E* is also seen on the NW trend map, where the anomalous fault population of this trend is almost non-existent within this fault set. This is also observed on the subsidiary trend map WNW. The effect of this fault set on the NE trend map is however represented by the sundering of the two NNE clusters of faults.

Among the fault sets discussed so far, it was shown that the NE *fault set B* and the NS *fault set E* both have controlled the distribution of all the other trends in the area (compare with fault map, Fig. 4).

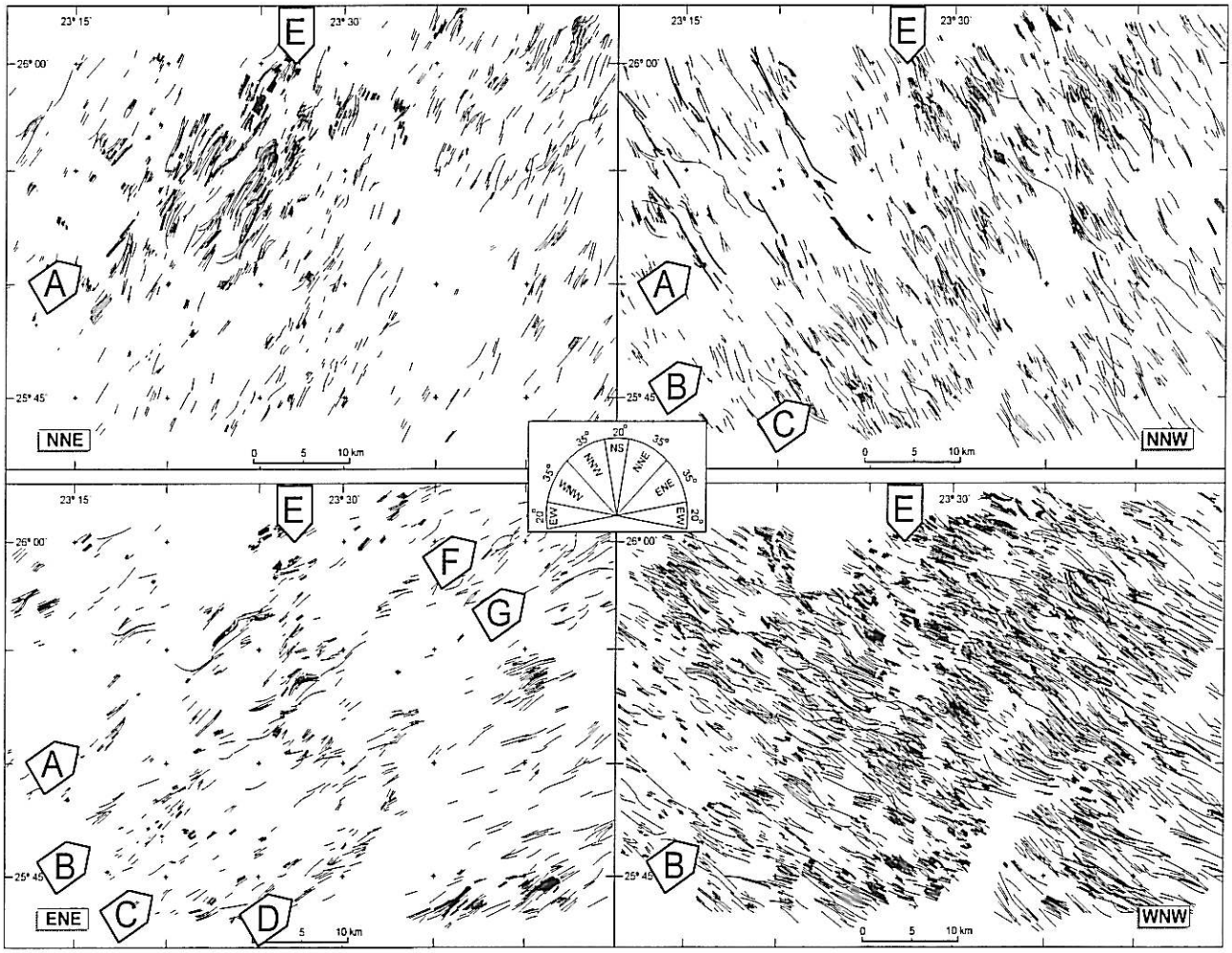

Fig. 6. Subset trend maps filtered from NW and NE trend maps (Fig. 5) through the template shown in centre.

The fault population in most of the trend maps is higher east of *fault set E*, as was described for the *fault set B*. This control indicates that both of these fault sets are among the first structural trends to have developed and should help in explaining the structural framework of the area.

Fault Sets F and G

These two northeast-trending fault sets are very important because they enclose between them a very peculiar cluster of curved faults displaying a crude "S" shape which have the same NE trend (Fig. 5). Both of these fault sets are not visible on the NNE trend map of fig. 6 because they belong to the ENE trend, therefore they would belong structurally to *fault sets* A to D.

Fault Sets H and I

These two northwest-trending fault sets define the limits of a large sigmoidal structure (highlighted on NW trend map, Fig. 5), which does not show on both the NNW and WNW trend maps. This indicates that it was formed from the combination of both of these two trends, where the smaller lozenge structures within the large sigmoidal structure are defined by two NNW and two WNW faults. The controlling effect of fault sets H and I is very prominent over the northeast fault sets, where *fault set H* is found to limit the continuation of fault sets A to D northeastward, while *fault set I* prevents fault sets F and G from extending southwestward (see NE trend, Fig. 5).

Structural Trends

Further enhancement of these fault sets was achieved by producing 22 more trend maps through permutational coupling of the original eight trend maps of figures 5 and 6, which brought the total number of trend maps to 30. These new maps emphasised the fault sets of figures 5 and 6 by bringing out new clusters of faults directly related to these fault sets.

The combination NE+NNW (Fig. 7 a) is presented here as an example. The intervening space between any two adjacent fault sets A to D shows distinctive fault patterns. These spaces are shown on figure 7 b as Belts 1 to 4, with the *NE Line* (or *fault set B*) as the median of these belts. Belt 1 and Belt 2 are represented by long and widely spaced NNW faults (highlighted on Figure 6, NNW trend) that either terminate or offset across *fault set A*. These same belts are also accentuated by the two NNE clusters of faults. Fault sets B and C mark the boundaries of Belt 3, where the NNW trend has closely spaced faults with their lengths defining the width of this belt. While Belt 4 has the least distinctive pattern of faults, the scattered orientation of the faults in this belt gives a contrast against Belt 3, which further help define the limits of both belts. All four of these belts stop abruptly at *fault set H* (Line 1, Fig. 7 b).

Graben1 and Graben 2 (*fault set E*) represent a north-south, right-stepping *en echelon* set of grabens (stippled on Fig. 7 c) with the southern segment extending farther south beyond the area of figure 7 a. As was discussed earlier, this *en echelon* set was found to affect most of the structures described thus far.

Kinematic Settings

The four belts are believed to represent the width of a northeast-trending wrench system –about 30 km wide– with the *NE line* as the median of this system (Fig. 7, b) especially that most of the faults in the area are strike-slip faults having fault planes with clear horizontal grooves or slickensides.

A structural system of this nature and width must cover a much larger area than is defined by the limits of Jabal Al Qardabah Sheet. According to Aydin and Nur (1982), the length of a strike-slip system is three times its width. This would put the length of the assumed NE wrench system around 100 km, not to exclude the possibility that the wrench system at hand is part of a much wider system, which would put the length of such a wrench system in the order of hundreds or even thousands of kilometres.

Geographically, Az Zalmah area represents the northeastern flanks of Al Kufrah Basin, a basin which covers territory in four neighbouring countries with an aerial extent of more than 400,000 km^2. This makes Az Zalmah area a representative sample for a regional model regarding the structure of this wrench system as part of NE Africa. Such a model has to take into account the plate tectonic settings of Africa throughout its geologic history.

The stress regime associated with strike-slip systems assumes horizontal maximum ($ó_1$) and minimum ($ó_3$) principal stress axes and a vertical intermediate principal stress axis ($ó_2$). These strike-slip systems usually occur in conjugate sets having opposite sense of displacements (Wilcox *et al,* 1973;

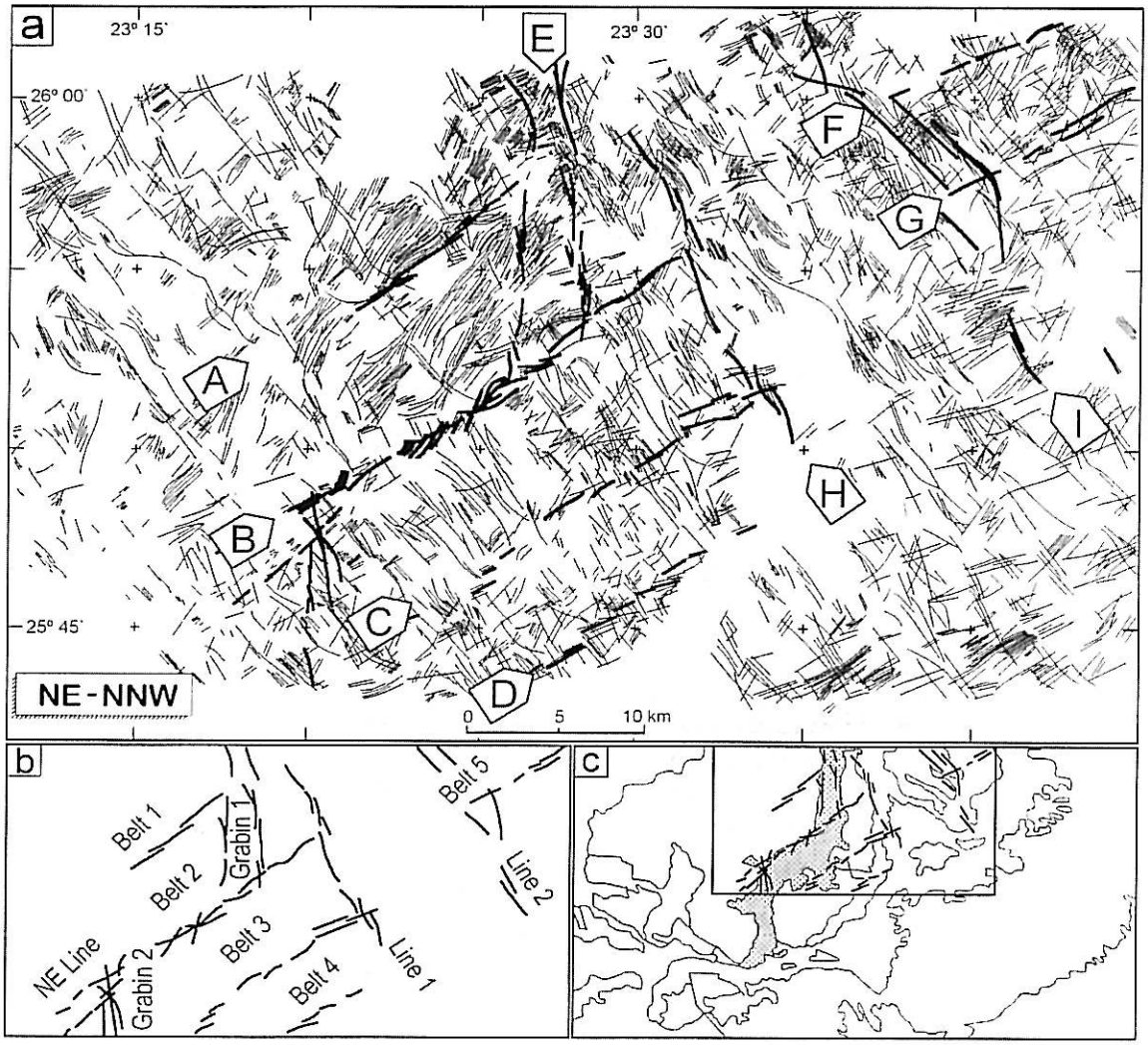

Fig. 7. (a). The combination of two trend maps bring out clear NE belts (b) marking wide shear zone. (c) Major belts relative to geological map (Fig. 2) and NS *En echelon* graben (slipped).

Ramsay, 1980). In Az Zalmah area, the maximum stress axis ($ó_1$) would assume a north-south orientation, representing the northward drift of Africa throughout the Phanerozoic, as postulated from several *Apparent Polar Wandering Paths (APWP)* for Gondwanaland (*e.g.* Morel and Irving, 1978; Scotese *et al*, 1979; Condie, 1982; Bachtadse and Briden, 1991). The conjugate set associated with this orientation would then assume a NE sinistral shear and a NW dextral shear. The tension fractures accompanying this setting would assume a north-south orientation, parallel to $ó_1$ (Fig. 9 d-1).

Rhomboidal fault-block structures are typical of *en echelon* faults within a strike-slip system. Depending on the *en echelon* sense (left- or right-stepping) and the sense of movement along the pair of strike-slip faults, pressure ridges and basins would develop in the area between the *en echelon* set in response to compression or extension, respectively (Wilcox *et al*, 1973; Aydin and Nur, 1982; Ramsay and Huber, 1987). Several of the fault-block structures which were visited in the field have a NW orientation (Fig. 8; see location of each structure on Fig. 2) ranging in size between 1 km ^{2} (Fig. 8 a) and more than 40 km ^{2} (Fig. 8 d), and depending on their size, large structures are bounded by relatively wide fault zones, while small structures are bounded by a single fault on each side.

Figure 8 a shows a NW left-stepping *en echelon* set of faults developing a pressure ridge, which could only develop from dextral strike-slip faults as shown kinematically. Fig. 8 b represents a horst with a left-stepping *en echelon* set, while fig. 8 c shows a small basin with a right-stepping *en echelon* set. Both of these structures are compatible with dextral strike-slip faults. Because wrench or shear zones usually occur in conjugate sets having opposite sense of displacements (Wilcox *et al,* 1973; Ramsay, 1980), it

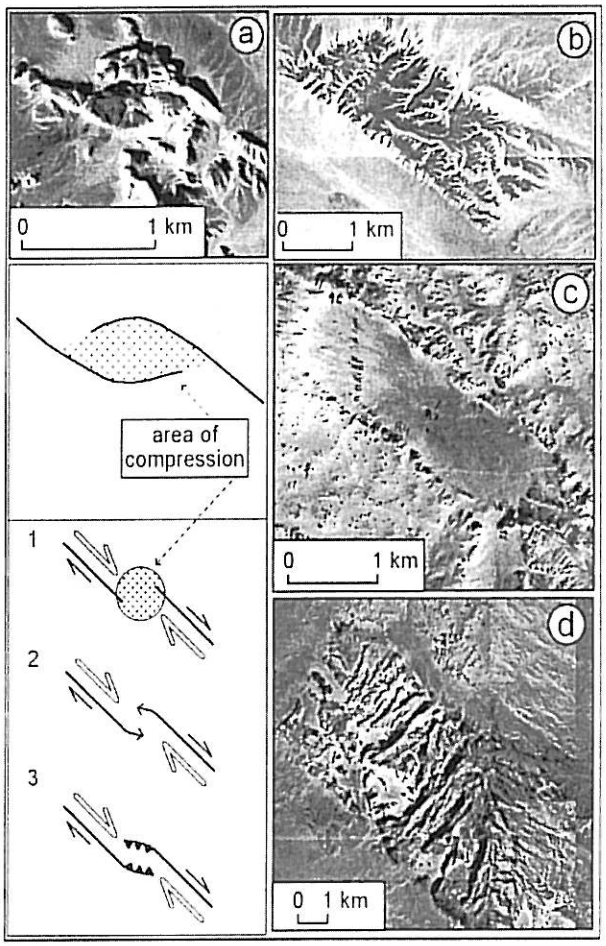

Fig. 8. Aerial photograph samples of structures found in the area. (a) pressure ridge caused by a left-stepping set of NW *en echelon* strike-slip faults. b, c and d: rhomboidal fault block structures, typical of a wrench system. See Fig. 2 for location of these structures.

is safe to assume that the NW trend represents the dextral antithetic component of the assumed wrench system (R_2 and X shears, see Fig. 9 d-1), whereas the NE fault sets and their associated belts–the throughgoing wrench system–would belong to the sinistral synthetic components, R_1 and P shears (Fig. 9 d-1).

If the proposed NE-trending wrench system were capable to move freely, the NE trend would have the highest fault population, and the fault-block structures (Fig. 8) would follow the same NE-trend. However, the NW trend, especially the WNW trend, is found to have the highest fault population, and the fault-block structures all have a northwestern orientation. Furthermore, while the NE-trending wrench zone with its four belts is wide enough to cause considerable lateral displacements, the NE faults show no such displacements as observed on the geological map of figure 2, nor have any of the faults visited in the field shown any appreciable displacement proportional to the width of the wrench zone.

This raises the possibility that the proposed wrench system might be inherently blocked. In clay model experiments (Tchalenko and Ambraseys, 1970; Wilcox *et al*, 1973) faults related to synthetic sinistral shear P (ENE faults in this case) start to develop only at an advanced stage of a wrench system, when the major fault is curved (Freund, 1974), which suggests that these faults, together with their complimentary set, the antithetic dextral shear X (WNW faults), emerge from the resistance of the main wrench system to any further movement. Freund (1974) considers interconnecting *en echelon* segments as one of the explanations for the curvature of a wrench system which causes the resistance of the main wrench system to any further movement.

The *en echelon* arrangement of tension fractures accompanying a shear zone is a good criterion in deciding whether the displacement along the shear zone is dextral or sinistral (Badgley, 1965; Billings, 1972; Wilcox *et al*, 1973). In our case, the north-south, right-stepping *en echelon* set of grabens (stippled on Fig. 9 b) are compatible with a sinistral NE-trending wrench system, whereas a dextral system would produce EW left-stepping *en echelon* grabens (Fig. 9 a).

Wilcox *et al* (1973), conducting clay model experiments simulating shear zones, state that: "*En echelon* tension fractures may form along a wrench zone in the initial stage of deformation, but they easily are destroyed as wrench displacement increases and compressive structures (folds and conjugate faults) become more prominent" (Wilcox *et al*, 1973, page 87). Two points in this statement are of great importance. Firstly, that tension fractures mark the initiation of a shear zone. We have shown that the different fault trends were either truncated or confined by *fault set E* (Figs. 5, 6, and 7). Such controlling effect of *fault set E* indicates that it was among the first structures to develop in the area, and the Upper Ordovician stratigraphic sequence filling this *en echelon* set of grabens give an estimated timing for their opening around Early to Middle Ordovician. Secondly, that tension fractures are destroyed after conjugate shears develop. Figure 9 **c** shows that the *en echelon* grabens filled by Melaz Shuqran and Mamuniyat formations must have been subjected to intense compression to develop the syncline-like structure it displays and to cause the alignment of Melaz Shuqran Formation along the margins of both segments of the *en echelon* set of

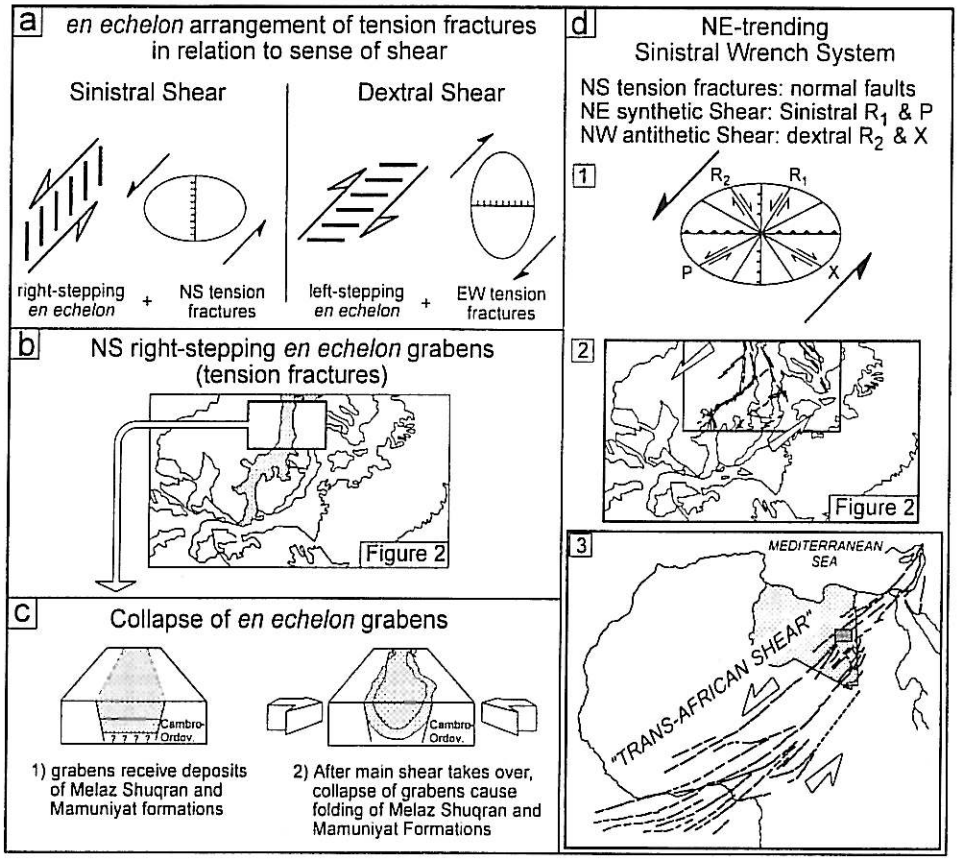

Fig. 9. A synopsis of the kinermatic interpretations for fault trends and the tectonic print over the stratigraphy in the area, See text for discussion e3 after Neev *et al* (1982).

grabens. Similar "folding" is nowhere found near these grabens, which indicates that this is a structural feature related only to these grabens. Furthermore, the axes of any regional folding associated with the northeast-trending shear zone at hand would assume an east-west trend, parallel to thrusts and reverse faults (see Fig. 9 d-1).

This NE configuration of the proposed wrench system could be part of the Trans-African Lineament (Nagy *et al*, 1977; Neev *et al*, 1982; Schandelmeier *et al*, 1997) which is a sinistral megashear system extending from the Benue trough of Nigeria via the Chad Basin and Al Kufrah Basin, into Egypt and the Levant, and terminating at the Anatolian fault in Turkey (Fig. 9 d-3).

MAGNETIC MAP

The existence of a northeast-trending wrench system in Az Zalmah area as was established earlier through the kinematic analyses of the structural trends and their relevant fault sets, as well as through the kinematic analyses of selected sample structures (Fig. 8) give a general picture for the tectonics in the area as it affected the geology on the surface, with no indication as to how the Precambrian basement was affected by the stress regime causing this wrench system.

A residual total intensity aeromagnetic map for Jabal Dalma area was published in 1980 by the Industrial Research Centre, Tripoli (see reference list). The magnetic map presented here (Fig. 11) is part of the surveyed area (see Index Map, Fig. 10). Both the geological map (Fig. 2) and the magnetic map cover exactly the same area, which would allow a three-dimensional correlation between the surface geology and the basement "topography".

Properties of a Magnetic Map

The magnetic contours, in gammas, represent the residual total intensity geomagnetic field relative to the theoretically calculated international geomagnetic reference field of 1975. The survey was carried at 122 ± 24 meters of ground clearance, with flight-line spacing of 1 km and tie line spacing of 5 km. This process of obtaining the residual field produced a contour map with an anomalous magnetic field. In

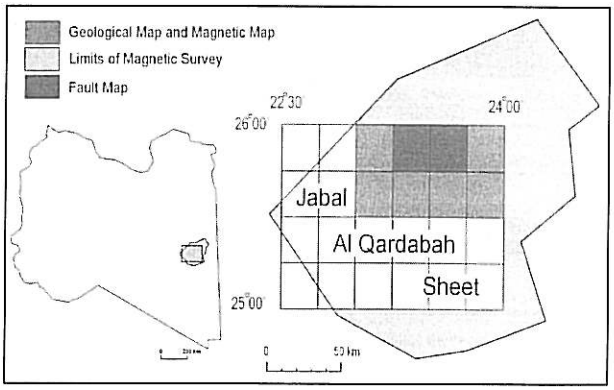

Fig. 10. Index map showing the area covered by the magnetic survey. Note that the area covered by magnetic map (Fig. 11) is the same as that covered by the geologic map (Fig. 2).

that sense it should be possible to interpret the magnetic map (Fig. 11) in terms of the structural and geological features causing the anomalous field, which should help in obtaining information about the subsurface geology of the area.

Particular properties regarding the magnetic survey operations and the magnetic map itself is important in enhancing the quality of the magnetic map and thus in utilising it as a qualitative tool in interpreting the configuration of the granitic basement. The first of these properties is the very low altitude of 98 to 146 meters at which the aeromagnetic survey was conducted. This should help in showing more sharply defined and better-resolved magnetic anomalies. Secondly, the clarity of the aeromagnetic survey and the sharpness of the anomalies are best achieved when the flight-line direction is normal to the trend of the geologic strike (Dobrin, 1976), as opposed to complicated anomalies arising from flight paths which make an oblique angle with the geologic strike. This criterion is fulfilled in the magnetic map presented here as the geologic map of figure 2 shows that the stratigraphic strike has a general northeast trend, while the direction for the flight-lines run along a N 35° W direction. And finally, the relatively small flight-line spacing of 1 km would also help in producing sharp and well-defined anomalies.

The magnetic map could be divided into three distinct zones: a North-western zone, a central zone, and a south-eastern zone (Fig. 11, insert).

North-Western Zone

Shows localised anomalies with high amplitudes and narrow wavelengths. These anomalies could represent shallow Precambrian intrusions or ferruginous Palaeozoic rocks. Within this zone, anomalies X1 and X2 (Fig. 11, insert) are the most prominent anomalies. These are the only two anomalies showing a northwestern trend. Structurally, anomaly X1 has a magnetic low and a clear right-stepping structural form, while X2 represents a magnetic high and a left-stepping structural form.

Central Zone

Sub-zone A is marked by a clear north-eastern alignment of closely-spaced contours, with its north-western and south-eastern limits taken at -200 gammas. The contours in the central "valley" of this sub-zone become less dense and reach -400 gammas,

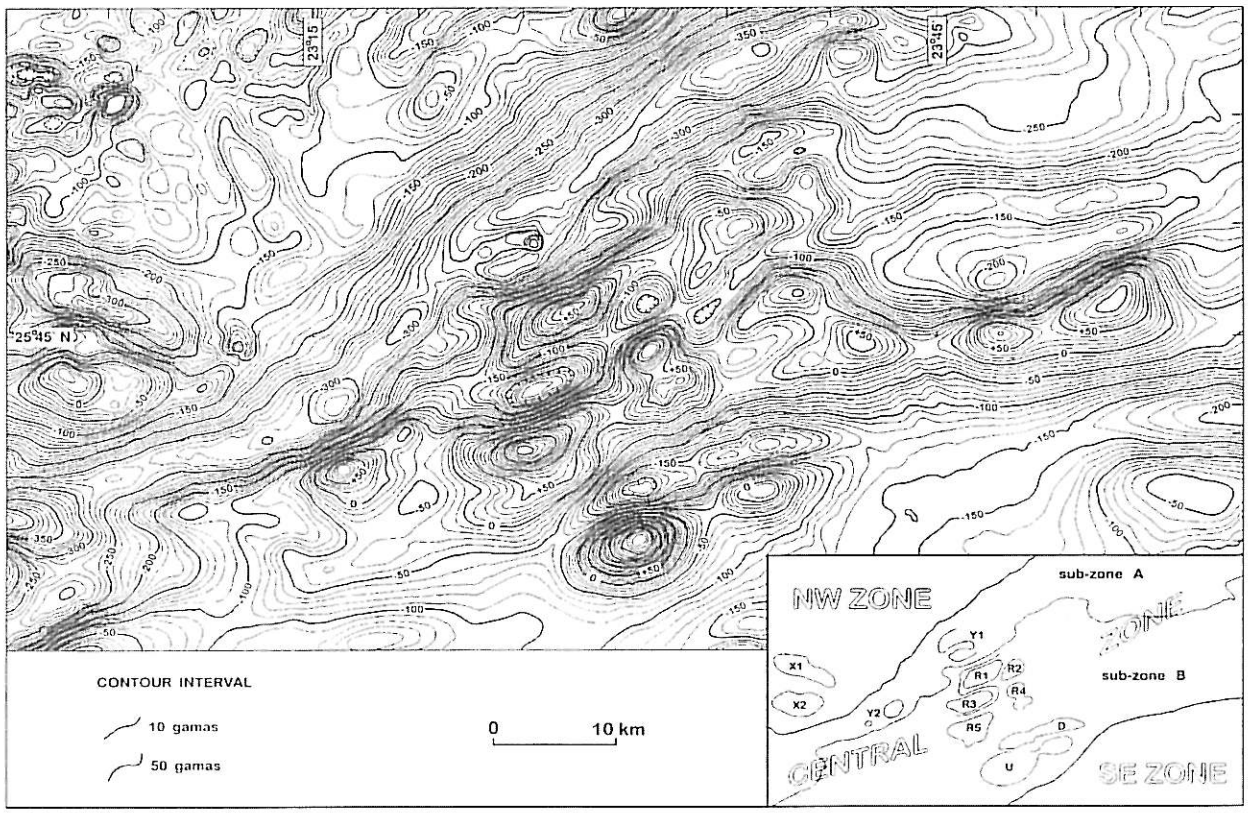

Fig. 11. A residual total intensity aeromagnetic map for part of Jabal Dalma area (Jabal Al Qardabah Sheet). Anomalous zones are given in inset, as well as individual anomalies discussed in text. See Fig. 10 for location of map with respect to mgnetic survey area.

the lowest in the area. Along the length of sub-zone A, the contours alternate in their linear trend between ENE and NNE directions. The two points at which this change in direction takes place are marked by Y1 and Y2. At Y1, the contours follow clear east-west closures, while at Y2 the contours form adjacent circular depressions that are offset along an east-west trend. East of longitude 23°40'00", the contours of sub-zone A are widely spaced and no longer have their distinct north-eastern alignment, probably reflecting increased thickness of sediments.

Within sub-zone B, the anomalies labelled R1 to R5 are bounded by conspicuous trends orientated ENE and NNE. Combined together, these trends form well defined rhomb-shaped "blocks" (especially anomaly R1) with values alternating between highs and lows, probably reflecting corresponding basement topography. Towards the southern limits of the central zone, anomalies U and D show a left-stepping form along an ENE trend, with anomaly D representing a magnetic low, while anomaly U a magnetic high of more than +250 gammas, the highest in the area.

South-Eastern Zone

The limits of this zone with the central zone is taken along an arbitrary line across which the contour spacing becomes markedly open. As this zone is closer to the centre of Al Kufrah Basin, the widely spaced contours and subdued anomalies could be due to the increased thickness of the sediments. Despite the subdued anomalies, the contours still retain their overall north-eastern trend.

Magnetic Anomalies

The three zones described above have been delineated according to the distribution of the individual magnetic anomalies marked in the insert of figure 11. These anomalies are believed to reflect the structural manifestation of the wrench system on the magnetic "basement". Figure 12 shows the relationship between the magnetic map and the structural trends deduced from the fault map (Fig. 4) and its filtered trend maps (Figs. 5 and 6). Among other correlative features between the structural trends and the magnetic map, the NE Line marking the median of the shear zone is the most striking of these features, where it coincides exactly with the central valley of sub-zone A (Fig. 12). This indicates that there is a direct correlation between the structure as it is seen on the surface, and the granitic basement as reflected by the magnetic map. As such, the magnetic anomalies could be interpreted within the context of the proposed structural model of the northeast-trending wrench system.

Anomalies X1 and X2

Within the area of figure 11, these are the only two anomalies which have a NW trend. When these two anomalies are viewed within the geological framework in the area, it can be seen that anomaly X1 corresponds structurally to a graben represented by Upper Ordovician units, while anomaly X2 lies beneath a horst represented by Cambrian–Lower Ordovician units (Fig. 13, a). Corresponding 'grabens' and 'horsts' are also seen on the magnetic map, where anomaly X1 represents a magnetic low, and X2 represents a magnetic high.

By applying the proposed mechanical model (Fig. 9, e-1) anomaly X1 could be resulting from the interaction between the north-south normal faults and the WNW antithetic X-faults (see Fig. 13, b). Structurally, the northern limits of this anomaly is represented by a right-stepping set of dextral faults

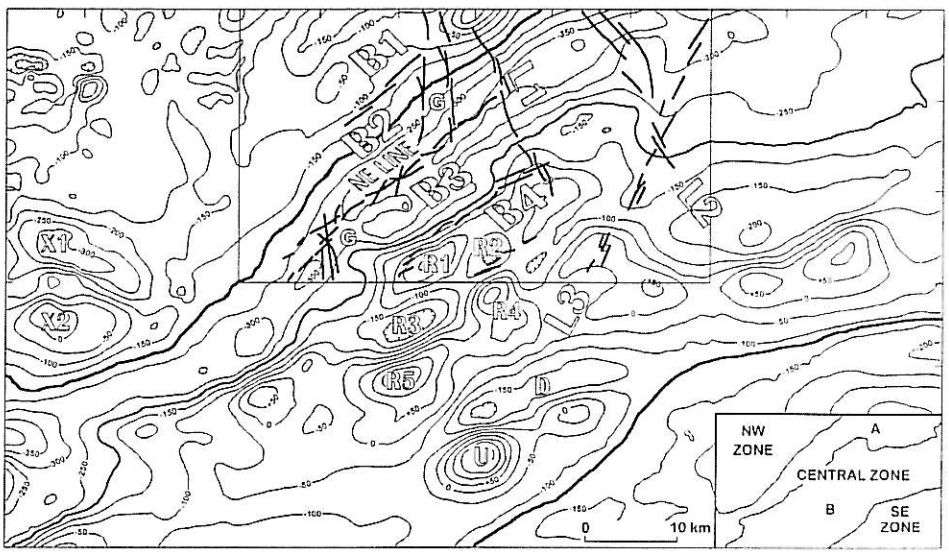

Fig. 12. Relation between structural trends associated with proposed wrench system deduced from fault map (Fig. 4, see also Fig. 7.) and magnetic map (Fig. 11).

joined by a north-south normal fault (Fig. 13, c). Such a configuration would create an extensional stress system, leading to an ideal pull-apart basin.

Anomaly X2 (Fig. 13, d) is interpreted as bounded on its northern limits by a left-stepping set of dextral X-faults joined by a NE sinistral fault which could belong to either R_1 or P-faults. This fault set develops a compressional state of stress. The other three faults bounding this anomaly would add to this compressional state of stress, where the northern and southern corners of this structure are subjected to compression, while the eastern and western corners are subjected to extension. Combining these kinematic conditions would lead to an overall counterclockwise rotation of the whole block, which would add to the compression exerted on this structure, thus causing it to be uplifted.

The two anomalies X1 and X2, with their corresponding graben and horst on the surface, are well related mechanically to each other in the sense that the extension developing in X1 would induce compression on X2 and *vice versa* . This could of course be related from a geophysical point of view to the dipole effect of magnetic anomalies, but since the magnetic map is a residual one, the anomalies are enhanced by the removal of the regional, therefore these anomalies are representative for fault block structures especially that they are bounded by elongated or linear zones of steep magnetic gradients suggesting faulted and displaced magnetised blocks (Dobrin, 1976).

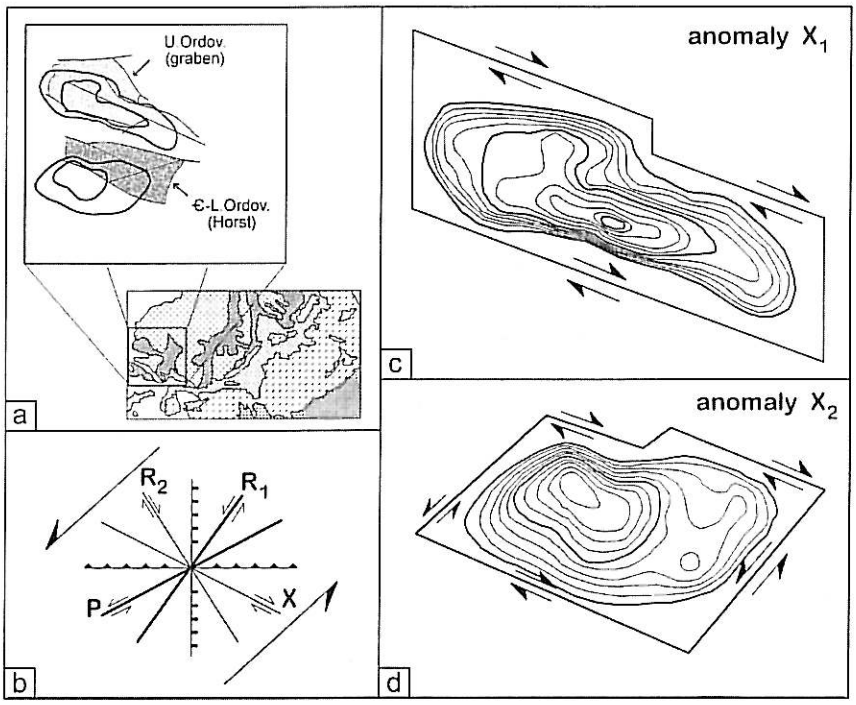

Fig. 13. Applying mechanical model to magnetic anomalies X1 and X2, a: location of anomalies relative to NW-trending structures on geologic map (Fig. 2), b: mechanical model, c: kinematics of anomaly X1, d: kinematics of anomaly X2.

Anomalies R1-R5

These anomalies (for location see Figs. 12 and 14, a) are found beneath the highly displaced outcrops of Melaz Shuqran Formation just to the east of the southern segment of the right-stepping *en echelon* set of grabens. In fact, the whole area above these anomalies is the most fractured part of the geological map of figure 2. These anomalies are believed to be the result of the interaction between the synthetic sinistral shears R_1 and P. Combined together, these faults would create lozenge-shaped structures with an overall east-northeast direction. As figure 14 c shows, these structures start with the development of a series of right-stepping sinistral faults R_1. Due to geometrical restrictions, the P-faults cannot operate simultaneously with the R_1 faults, rather only in sequence since they both belong to the same conjugate set (Freund, 1974). This will create the lozenge-shaped structures (stage 2, Fig. 14 c) which will be subjected to clockwise rotation (stage 3) since they are bounded by sinistral faults on all sides. These duplex structures have a contractional geometry and are imbricated by P shears between pre-existing R shears (Woodcock and Fischer, 1986, Fig. 7 c). Once they start to develop progressively, each unit lozenge would rotate independently, forcing the neighbouring lozenge to absorb part of the stress exerted upon it, and *vice versa*. The progressive development and rotation of these blocks would create volume excess at restraining edges and volume deficit at releasing edges of the lozenge or rhomboid blocks making up this duplex structure. To accommodate for these volume changes, the mechanical system necessitates the discrete uplift and subsidence of the individual blocks in an alternating fashion. This is clearly seen on the magnetic map, where anomalies R1, R4, and R5 are uplifted blocks, while anomalies

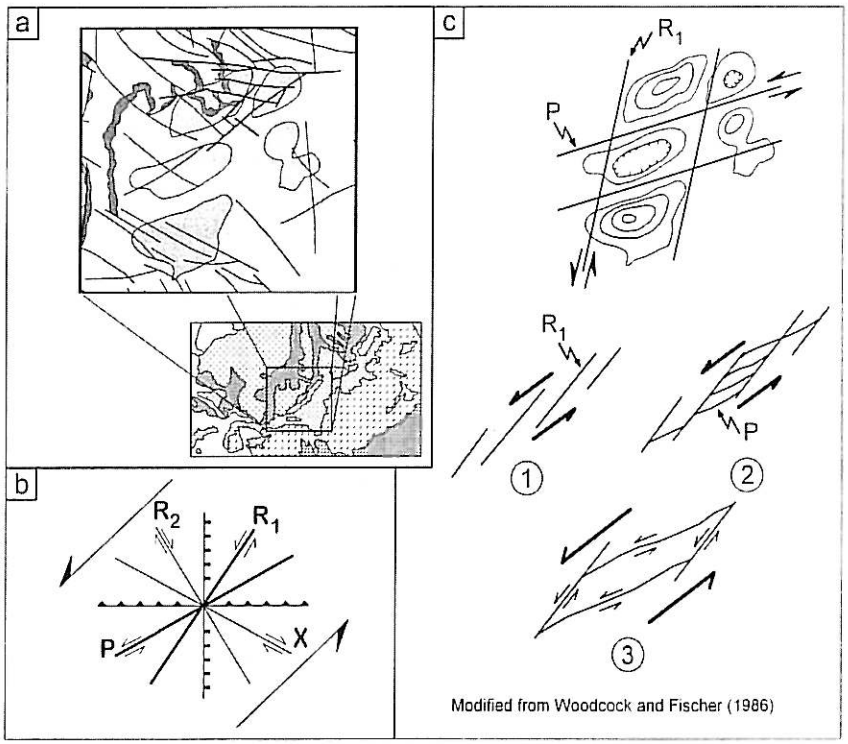

Fig. 14. Applying kinematic model to magnetic anomalies R1 to R5. a: location of anomalies relative to geologic map (Fig. 2.). b: kinematic model. c: interpretation of mechanical development of anomalies.

R2 and R3 are down-thrown blocks. It should be pointed out that while the internal rotation within each block is clockwise, the external rotation (heavy arrows in stages 1-3, Fig. 14 c) is counterclockwise, the latter of which represents the proposed shear system and represented by the outer arrows in figure 14b. This could further explain the limited volume change created by the rotation of the individual blocks, where the outer rotation would counterbalance this volume change and even help the whole duplex system to reach equilibrium by allowing the uplift and subsidence of the individual blocks.

Anomalies D and U

These two anomalies lie beneath Devonian rocks on the geological map (see Fig. 15 a) and are among the anomalies found within sub-zone B on the magnetic map (Fig. 12). They are both bounded by ENE left-stepping sinistral faults and NNE right-stepping sinistral faults (Fig. 15 c). These two structures are created by P-faults (ENE) isolating lozenges already cut by R shears (NNE). In this setting they would have an extensional geometry (Woodcock and Fischer, 1986, Fig. 7b). Anomaly D is cut into three lozenges and has a clear extensional form as seen by the negative magnetic contours. Anomaly U, on the other hand, has positive magnetic contours, the highest within the area of figure 11, which would suggest a contractional geometry. It will be shown later that in spite of the positive magnetic contours of anomaly U, it still represents the extensional geometry associated with the model of figure 15 c.

The locked fault structure (Fig. 8, a) which is also a duplex structure made up of one lozenge, is located above the two anomalies U and D (Fig. 15, d). These two anomalies and the anomalies R1-R5, discussed earlier, seem to be associated with very complex structures on the surface. This is probably resulting from the rotation of individual blocks making up these anomalies, as well as the vertical movements of these blocks in association with this rotation.

Sub-zone A: Central Valley

One of the striking features of the magnetic map (Fig. 11) is the linearity of sub-zone A with contours starting at -150 gammas and reaching -400 gammas, which from a structural point of view represents a very deep valley. This *central valley* (Fig. 16) displays a very peculiar pattern in which the contours deviate from their northeast alignment at points Y1 and Y2 (Fig. 16) to become aligned along an east-west closer, as at Y1, or marked by an east-west offset at Y2. This overall configuration gives the central valley a distinct right-stepping *en echelon* setting. This *en echelon* setting is highlighted by the hatched line along the centre of the valley in Figure 16, but could be viewed just as well on the magnetic map of Fig 11.

The location of the *NE-Line* exactly on this valley (Fig. 12) supports its *en echelon* setting, thus allowing for the line drawn on figure 16 along the central valley to represent a sinistral shear system. Such a configuration will build compressional force at the joining segments of the right-stepping *en echelon* (Fig. 16, a). Within the framework of the proposed shear system, the dominance of the NW trend–especially the WNW trend–was attributed to a locked shear system. A sinistral, left-stepping *en echelon*

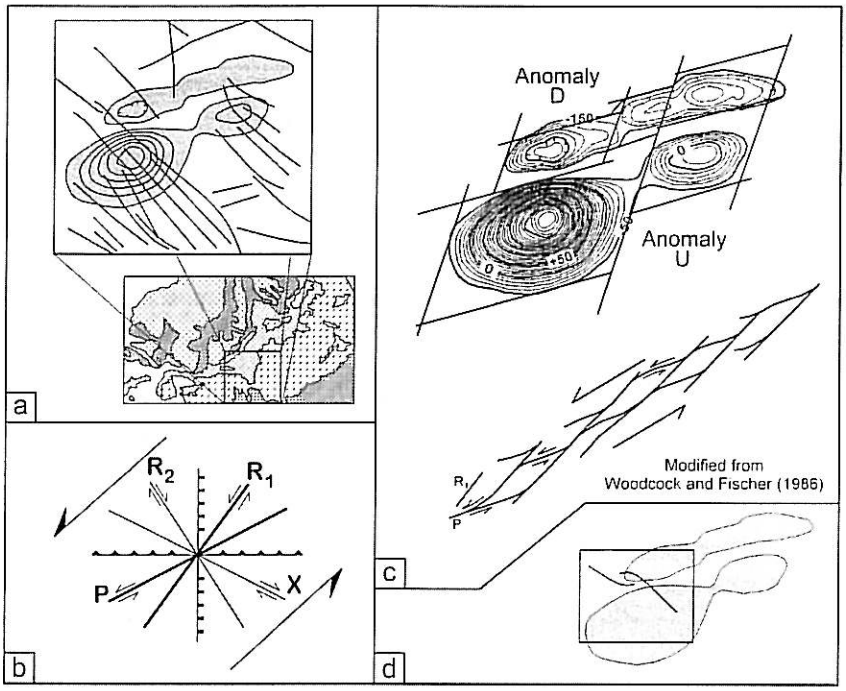

Fig. 15. Applying kinematic model to magnetic anomalies U and D. a: location of anomalies relative to geologic map (Fig. 2). b: kinematic model. c: interpretation of mechanical development of anomalies. d: location of anomalies relative to locked fault (Fig. 8, a).

system (Fig. 16, b) does not follow the contours of the central valley on the magnetic map, nor does it fit with the dominance of the NW trend in the area.

Sub-zone B: En echelon Folds

En echelon folding is cited in the literature as an indication for the existence of a wrench system even if no clear fault system is observed (*e.g.* Campbell, 1958; Wilcox *et al*, 1973; Harding, 1974; Harding and Lowell, 1979; Reading, 1980; Allen and Allen, 1990; Schandelmeier *et al*, 1997). The axes of these *en echelon* folds are found at right-angels to the direction of the maximum principal compressive stress ($\acute{o}_1$) causing the shear system (see Fig. 9,d-1).

The stepping of these *en echelon* folds is an indication for the sense of movement of a northeast-trending shear system causing these folds: left-stepping *en echelon* folds are associated with a left-lateral or sinistral shear system; right-stepping *en echelon* folds are associated with a right-lateral or dextral shear system. Figure 17 shows the possible orientation of such folds in the area, relative to a northeast-trending wrench system, given as either sinistral or dextral (Fig. 17, A and C, respectively). In the case of a sinistral wrench system, the *en echelon* folds have east-west fold axes, while the dextral wrench system will develop north-south fold axes.

Two corresponding world examples are given for comparison. The Dead Sea rift, a north-south sinistral strike-slip fault system (Quennell, 1959), shows left-stepping *en echelon* folds with northeast axes (in

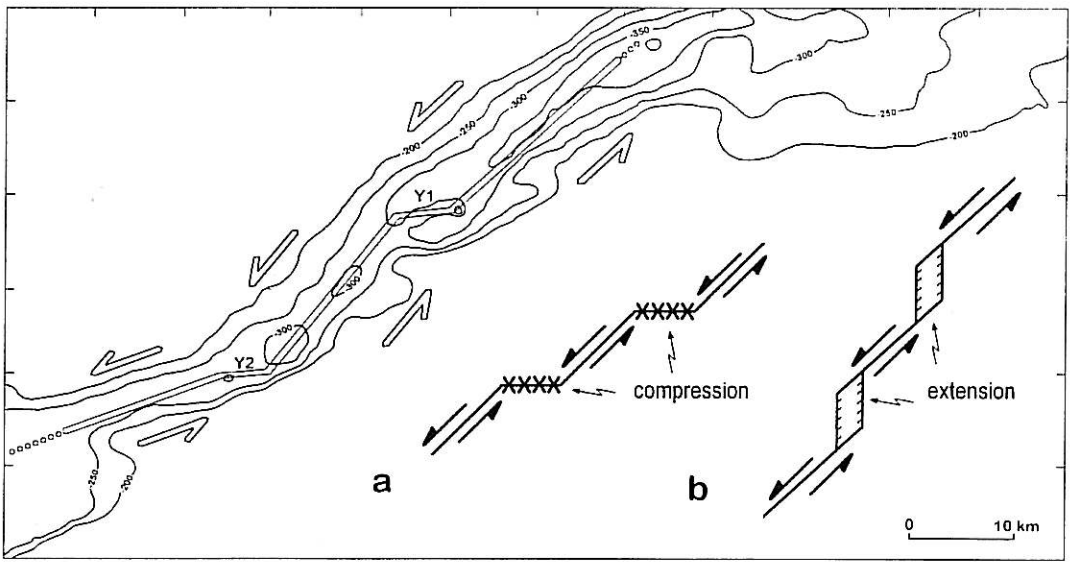

Fig. 16. The central valley within sub-zone A, interpreted as a sinistral shear system with a right-stepping *en echelon* set (a), where the compression (xxx) explains why this system is a "locked" system, dominated by P and X shears (NW faults). A left-stepping configuration (b) does not agree with the magnetic map nor with the dominance of P and X shears.

Fig. 17 B it is orientated to match the case in A, the study area). The San Andreas dextral wrench system, with its north-west trending main strike-slip fault (Fig. 17, D), has right-stepping *en echelon* folds with their axes trending at about west-northwest (Fig. 17 D, this is also orientated to be aligned with the case in C).

Between cases A and C, figure 17, the expected orientation of these folds would be that of case A since this setting, based on the structural information gathered so far, is identical to the structural model proposed (Fig. 9, d-1). Sub-zone B (Fig. 11) could be viewed as representing a set of east-northeast, left-stepping *en echelon* folds. The proposed *en echelon* folds are highlighted on figure 18 A by a 5 gamma contour interval on the background of the magnetic map with a 50 gamma contour interval. These folds are seen as anticlines and synclines with an east-northeast plunge (Fig. 18 b). The plunge of the individual folds is accompanied by a flatter overall plunge. This association between individual and regional plunge is in agreement with one of four possibilities given by Campbell (1958) for *en echelon* folds in the Kalgoorlie district in Western Australia. The four possibilities are based on the direct relationship between the *en echelon* pattern of folds (whether left-stepping or right-stepping) and the *en echelon* pattern of structure contours drawn on such folds (also being either left-stepping or right-stepping). In our case, the conditions are as follows: left-stepping *en echelon* folds in association with left-stepping contours will result in steep individual plunge of folds within a flat overall or regional plunge. These conditions are fulfilled, as seen in figure 18, where the *en echelon* pattern of the folds is clearly left-stepping, and if one is to draw structure contours on top of these folds, they will clearly show a left-stepping pattern (compare between the contours of more than 200 gammas at the western part of anomaly U, figure 15, with those of 0 gamma at the eastern end of the same anomaly). Figure 18 C is the model given by Cambell to show the relation between individual and regional plunge. Although it represents flat individual plunge within a steep regional plunge, whereas the case proposed here is the combination of steep individual plunge with flat overall plunge, nevertheless, this three dimensional model serves the purpose where it is orientated to resemble the configuration of the folds seen on the magnetic map (Fig. 18 a).

It should be pointed out that anomalies R1-R5 (Fig. 14) and anomalies U and D (Fig. 15) described earlier, are part of the *en echelon* folds discussed here. While these anomalies were described in the context of lozenges cut by R and P shears, they can still be part of the *en echelon* folds discussed here. Both structural events (folding and faulting) can be

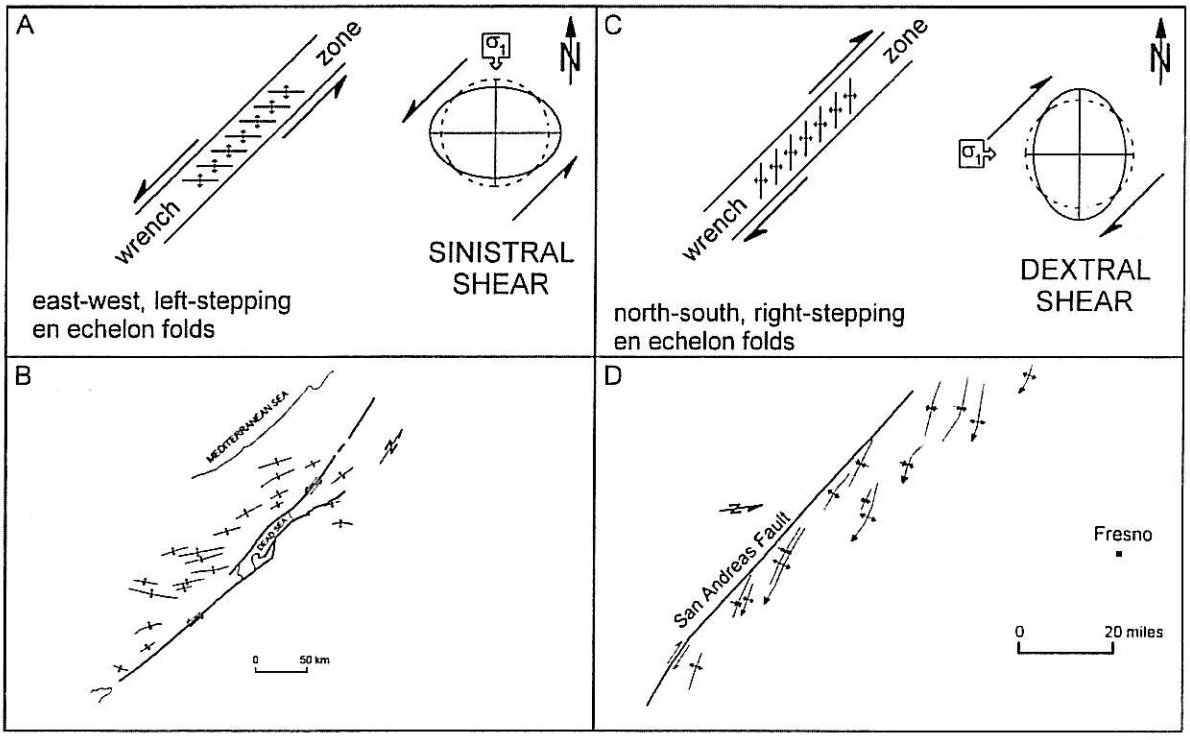

Fig. 17. The alignment of *en echelon* folds in a predicted orientation depending on the wrench system being A: sinistral or C: dextral. B: The Dead Sea Rift System (modified from Quennell, 1959). D: The San Andreas Fault System (modified from Wilcox *et al*, 1973.

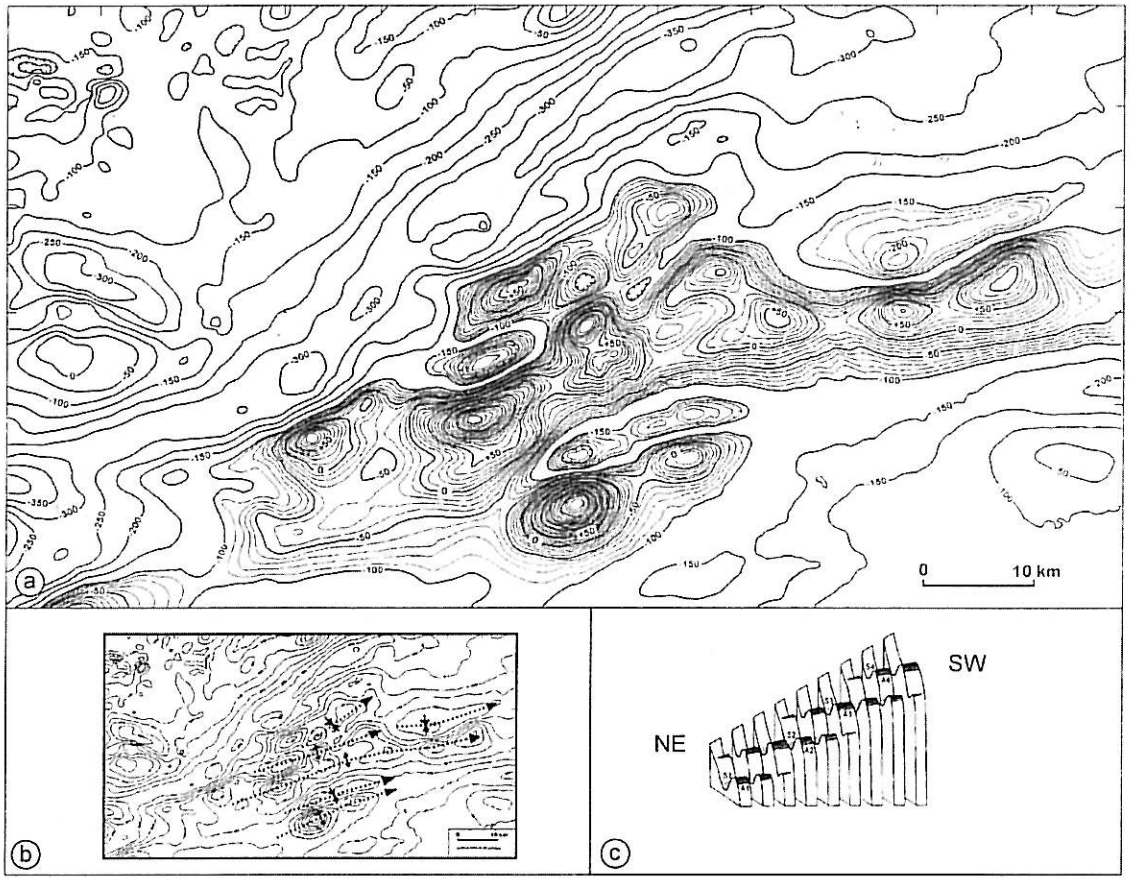

Fig. 18a. Sub-zone B, highlighted to show the possible *en echelon* configuration of folds in the basement in response to the kinematic model proposed. B: Trends of fold axes showing plunge to east-northeast. C: A 3D representation of folds, modified from Cambell (1958).

accommodated for within the framework of the proposed mechanical model. A pertinent example is given by Harding and Lowell (1979) for the evolution of a wrench fault developing hydrocarbon trapping, modelled after examples in California. This example is presented in figure 19 to match the case for a sinistral wrench system, which is the case in Dalma area (Survey area, see Fig. 10) while the original California example is that of a dextral wrench system. It can be seen that the initial stage creates connected *en echelon* folds (Fig. 19 A). At a later stage, and while the axes of these folds continue to extend east-west, the crests of these folds are cut by sinistral faults having either left-stepping or right-stepping *en echelon* patterns (Fig. 19 B). At a more advanced stage (Fig. 19 C) the folds are dissected by the sinistral faults, for which these faults will join together to form either rhomboid horsts or grabens, depending on the *en echelon* offsets they have.

There is a direct relationship between the structural setting of a wrench system and the hydrocarbon accumulation within the closures at the crests of the *en echelon* folds. This is shown by the

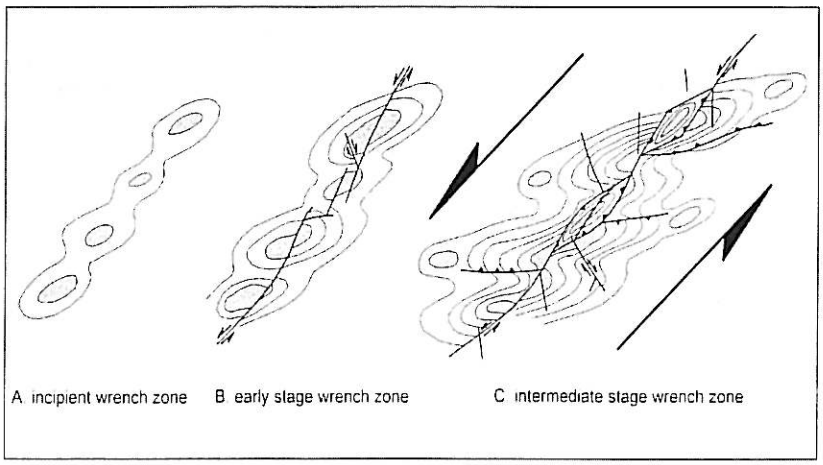

Fig. 19. The revolution of a wrench system, developing *en echelon* folding followed by faulting which will create lozenge or rhomboid structures. Shaded regions represent potential hydrocarbon traps within closures in fold crest modified

shaded closures in figure 19, where they represent the ideal hydrocarbon traps, being isolated at the highest levels of the structures and sealed by faults at predicted levels and orientations. This model is in good agreement with the *en echelon* fold pattern shown on figure 18, as well as with the kinematic layout given for the magnetic anomalies R1-R5 and both D and U anomalies. With the assumption that the magnetic map and all the structures deduced from it being that of the granitic basement, and if such *en echelon* folding in this basement is transmitted to the sedimentary cover, then the model proposed here could be adopted for hydrocarbon exploration in the area, where it could prove to be productive.

While most of the structural trends identified on the surface were shown, from the qualitative evaluation of the magnetic map, to have conforming structural influence at the "basement" level, the north-south *en echelon* set of grabens (stippled on Fig. 7 c) had no print on this basement (this is clearly seen on Fig. 12), despite their profound impact on the distribution of faults in all the filtered trend maps. According to the mechanical model of figure 9 d-1, the structural trends defining Graben 1 and Graben 2 (Fig. 7 b) belong to the north-south normal faults of that model. These are the tension fractures of Wilcox *et al* (1973), and according to their clay cake experiments, these tension fractures are short-lived and only develop at the early stages of wrenching, if they develop at all. Accordingly, these *en echelon* grabens are not expected to extend vertically to the depth of the granitic basement, firstly because they develop during the early stages of wrenching, they are easily taken over by folds and conjugate faults, and secondly, these same folds and conjugate faults will build up compressive stresses which will seal the walls of these *en echelon* grabens and will not allow them to extend vertically beyond the shallow depths of the crust, hence they will arguably not show on the magnetic map. This is a supporting evidence for the nature of the *en echelon* set of grabens in the area as discussed under *Structural Framework*, and a conformation for the mechanical model (Fig. 9 d-1) proposed for the area.

REFERENCES

Allen, P. A. and Allen, J. R., 1997. *Basin Analysis: Principles and Applications*. Blackwell Scientific Publications, Oxford. 441 p.

Aydin, A. and Nur, A., 1982. Evolution of pull-apart basins and their scale independence. *Tectonics*, **1**, 91-105.

Bachtadse, V. and Briden, J. C., 1991. Palaeomagnetics of Devonian ring complexes from the Bayuda Desert, Sudan: new constraints on the apparent polar wandering path for Gondwanaland. *Geophys. J. Intern.*, **104**, 635-646.

Badgley, P. C., 1965. *Structural and Tectonic Principles*. Harper & Row, New York. 521 p.

Bellini, E. and Massa, D., 1980. A stratigraphic contribution to the Palaeozoic of the southern basins of Libya. In: M. J. Salem and M. T. Busrewil (eds.) *The Geology of Libya*. Academic Press, London, **I**, 3-56.

Billings, M. P.,1972. *Structural Geology*. Prentice Hall, New Jersey. Third Edition. 606 p.

Campbell, J. D., 1958. En echelon folding. *Econ. Geol.*, **53**, 448-472.

Condie, K. C., 1982. *Plate Tectonics and Crustal Evolution*. Pergamon Press, New York. 310 p.

Dobrin, M. B., 1976. *Introduction to Geophysical Prospecting*. McGraw-Hill, New York, 630 p.

Freund, R., 1974. Kinematics of transform and transcurrent faults. *Tectonophysics*, **21**, 93-134.

Harding, T. P., 1974. Petroleum traps associated with wrench faults. *Bull. Am. Assoc. Petrol. Geol.*, **58**, 1290-1304.

Harding, T. P. and Lowell, J. D., 1979. Structural styles, their plate-tectonic habitats, and hydrocarbon traps in petroleum provinces. *Bull. Am. Assoc. Petrol. Geol.*, **63**, 1016-1058.

IRC, 1980. Residual Total Intensity Aeromagnetic Map of Jabal Dalma Area; 1:250 000. 1980. Compiled by Pacific Aero Survey Co., Tokyo, Japan., *Industrial Research Centre*, Tripoli, Libya. Unpublished Rep.

Klitzsch, E. H., 1966. Comments on the geology of the central parts of southern Libya and northern Chad. *In:* J. J. Williams *(ed.) South-Central Libya and Northern Chad: a Guidebook to the Geology and Prehistory. Petrol. Explor. Soc. Libya*, 8th Annu. Field Conf., 1-17.

Morel, P. and Irving, E., 1978. Tentative paleocontinental maps for the early Phanerozoic and Proterozoic. *J. Geol.*, **86**, 535-561.

Nagy, R. M., Ghuma, A, and Rogers, J. J. W., 1977. A crustal suture and lineament in Northern Africa. *Tectonophysics*, **31**, T67-T72.

Neev, D., Hall, J. K., and Saul, J. M., 1982. The Pelusium Megashear System across Africa and associated lineament swarms. *J. Geoph. Research.*, **87**, 1015-1030.

Nettleton, L. L., 1976. *Gravity and Magnetics in Oil Prospecting*. McGraw-Hill, New York, 464 p.

Quennell, A. M., 1959. Tectonics of the Dead Sea rift. *Asociación de Servicios Geológicos Africanos 20th Internat. Geol. Cong.*, México, D. F., 1956, Actas y Tr., 385-405.

Ramsay, J. G., 1980. Shear zone geometry: a review. *J. Struct. Geol.*, **2**, 83-99.

Ramsay, J. G. and Huber, M. I., 1987. *The Techniques of Modern Structural Geology*, vol. 2: Folds and Fractures. Academic Press, London, 700 p.

Reading, H. G., 1980. Characteristics and recognition of strike-slip fault systems. *In* P. F. Ballance and H. G Reading (eds.) *Sedimentation in Oblique Slip Mobile Zones. Spec. Publ. Internat. Assoc. Sedimentol.*, Blackwell, Oxford, **4**; 7-26.

Schandelmeier, H., Stern, R. J., Reynolds, P.-O., and Abdel Rahman, E. M., 1997. The Late Neoproterozoic (Venidian, ca. 570 Ma). *In* H. Schandelmeier and P.-O. Reynolds (eds.) *Palaeogeographic-Palaeotectonic Atlas of North-eastern Africa, Arabia, and Adjacent Areas*. Balkema, Rotterdam., 5-13.

Scotese, C. R., Bambach, R. K., Barton, C., Van der Voo, R. and Ziegler, A. M., 1979. Paleozoic base maps. *J. Geol.*, **87**, 217-277.

Tchalenko, J. S. and Ambraseys, N. N., 1970. Structural analysis of the Dasht-e Bayaz (Iran) earthquake fractures. *Bull. Geol. Soc. Am.*, **81**, 41-60.

Wilcox, R. E., Harding, T. P., and Seely, D. R., 1973. Basic wrench tectonics. *Bull. Am. Assoc. Petrol. Geol.*, **57**, 74-96.

Woodcock, N. H., and Fischer, M., 1986. Strike-slip duplexes. *J. Struct. Geol.*, **8**, 725-35.